Enhanced Skin Effect for Partial-Element Equivalent-Circuit (PEEC) Models

Karen M. Coperich, Albert E. Ruehli, *Fellow, IEEE*, and Andreas Cangellaris, *Fellow, IEEE*

***Abstract*—In this paper, a skin-effect modeling approach is presented that is suitable for all frequency regimes of interest and therefore is most appropriate for transient interconnect analysis. Yet, the new formulation lends itself to a model that can be abstracted for use in conjunction with surface integral and finite difference-based electromagnetic tools for interconnect modeling. While a volume filament technique is not computationally feasible at high frequencies, where a fine discretization is necessary, the formulation that is presented avoids this difficulty by carefully casting the behavior of a conductor into the form of a global surface impedance, thus requiring fewer unknowns. Several examples illustrating the ability of the proposed model to accurately capture proximity and skin-effect behaviors will be shown. Interconnect resistance and inductance per-unit-length results are given and compared with those obtained using different models.**

***Index Terms*—Interconnects, transmission lines.**

I. Introduction

THE COMPLEXITY and the speed of electronic packages require the use of accurate electromagnetic modeling for effective high-speed interconnect design. Clock rates of several hundred megahertz and rise times on the order of 100 ps at the printed circuit board level are common today. The high end of the spectra of some of the associated time waveforms may extend into the gigahertz range. This makes the use of accurate skin-effect models necessary. Availability of complete skin-effect models is especially important for accurate loss and dispersion calculations in transient simulations where the current is uniformly distributed over the cross section during the flat portions of the signal, while a surface-like current distribution exists during signal switching. As a result, several skin-effect models are in use today for different applications. Some of the early research work on skin-effect modeling was by the authors of [1] and [2]. A much-explored area is a frequency domain skin-effect model for transmission line modeling of interconnects. Recent advances in this area, presented in [3] and [4], include surface formulation models based on Green's first identity. Here, we are concentrating on improving techniques for the partial-element equivalent-circuit (PEEC) models [5] for both the frequency and the time domains. Also, model order reduction (MOR) techniques have been employed in [6] for inductance-resistance (Lp, R)PEEC volume filament models in order to make the method more computationally attractive when a large number of discretizations is necessary to capture the skin-effect behavior at high frequencies.

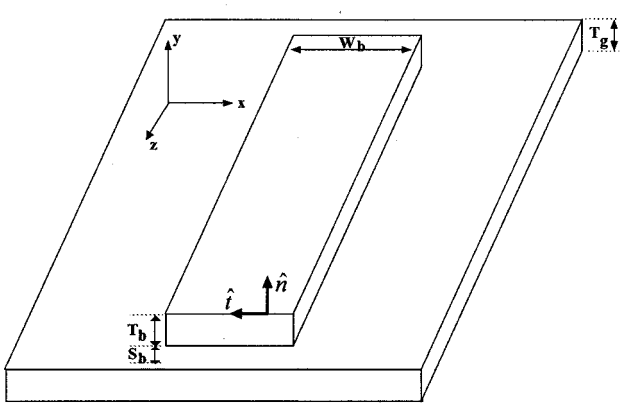

Fig. 1. Single conductive bar.

To motivate our approach, we consider the example geometry shown in Fig. 1 with a three-dimensional bar above a finite-size ground plane. In such a problem, several sources of skin effect are involved. The skin effect along the thickness of the plane and the bar, T_g and T_b, will occur at the highest frequencies.

If the skin depth δ at the maximum spectral frequency is smaller than the discretization h [as is the case for the current distribution in the conductor cross section of Fig. 2(a)], then a volume filament model may be too computationally costly for skin-effect modeling. For cases such as this, a surface-based method for skin-effect modeling is more cost effective than a volume-based method. However, the traditional surface impedance representation, $Z_s = (1 + j/s\delta)$, is effectively a local planar approximation. Currents at lower frequencies that permeate the conductor, like that shown in Fig. 2(b), are not accurately modeled by this surface impedance. It is also evident from Fig. 2 that such a local surface impedance model is not suitable for the accurate modeling of the effects of corners.

To address these modeling limitations, this paper pursues an approach that captures the frequency- and spatial-dependent behavior of the current distribution inside the conductors through the replacement of the high-frequency accurate local surface impedance model with a broadband global surface impedance (GSI) model. Sections II and III present the development of the global surface impedance model and its validation. Once the global surface impedance of a single conductor is generated, Section IV establishes the way it can be used in the integral equation formulation of the exterior electromagnetic boundary value problem for the prediction of the surface current distributions. Section V will illustrate how interconnect resistance and

Manuscript received June 15, 2000.

K. M. Coperich and A. Cangellaris are with the University of Illinois Urbana-Champaign, Urbana, IL 61801 USA.

A. E. Ruehli is with the IBM Research Division, T. J. Watson Research Center, Yorktown Heights, NY 10598 USA.

Publisher Item Identifier S 0018-9480(00)07409-3.

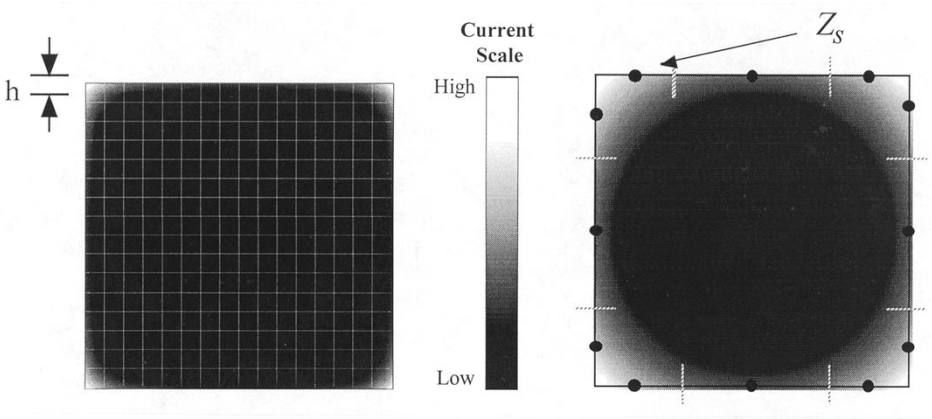

(a) (b)

Fig. 2. (a) Volume mesh: Inaccurately models the high frequency current distribution. (b) Local surface impedance model on a surface mesh: Inaccurately models the low frequency current distribution.

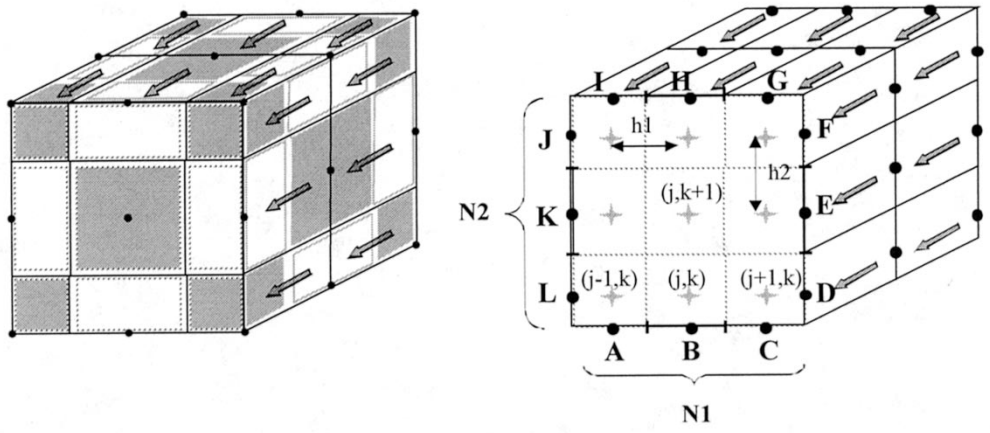

(a) (b)

Fig. 3. (a) Original PEEC mesh of a perfect electric conductor involving only surface unknowns. (b) Improved PEEC mesh of a lossy conductor.

inductance per-unit-length are computed using the new model and how they compare with results from other methods. Section VI will state the future directions of this work already underway.

II. The Proposed Model

For simplicity, consider the bar conductor shown in Fig. 1. Assuming that the current is flowing in the longitudinal direction, the electric field $\overline{E}$ has only the z-component $\overline{E} = \hat{z}E_z$. The equation governing the fields inside the conductor is the Helmholtz equation

$$\frac{\partial^2 E_z(x, y)}{\partial x^2} + \frac{\partial^2 E_z(x, y)}{\partial y^2} - s\mu\sigma E_z(x, y) = 0 \qquad (1)$$

where $s = j\omega$ is the complex frequency and μ and σ are the conductor's permeability and conductivity, respectively. The goal of improving lossy conductor models for the PEEC technique will be achieved by deriving a global surface impedance that preserves the physics of the interior of the *lossy* conductor while treating the unknown quantities of interest in the same manner as is done for the case of a *perfect* electric conductor. Namely, surface quantities are the only unknowns; there are no filament quantities in the cross section that must be solved for, as shown in Fig. 3(a).

In the improved PEEC model, the cross-section of the lossy conductor is separated into a finite-difference (internal) model, with unknowns at each of the "+" locations, while the surface cells constitute the external model, at each of the "•" nodes, as shown in Fig. 3(b). For uniform gridding, there are $N = N1 \cdot N2$ total internal nodes and $M = 2 \cdot (N1 + N2)$ surface cells. A two-dimensional (2-D) central difference approximation of the Laplacian operator applied at internal boundary cell (j, k) is given below after substitution in (1). For a corner cell, the operator will contain an additional $\partial E_z/\partial n$ term while analysis of an exclusively internal cell (such as cell $(j, k+1)$ in Fig. 3) will only contain values of adjacent neighbors $E_{z_{j\pm1,\,(k+1)\pm1}}$

$$\left[\frac{E_{z_{j+1,\,k}} - 2E_{z_{j,\,k}} + E_{z_{j-1,\,k}}}{h_1^2}\right] + \left[\frac{1}{h_2}\left(\frac{E_{z_{j,\,k+1}} - E_{z_{j,\,k}}}{h_2} - \left.\frac{\partial E_z}{\partial n}\right|_B\right)\right] - s\mu\sigma E_{z_{j,\,k}} = 0. \qquad (2)$$

The interior unknowns are the values of E_z at the N nodes, $E_{z_{j,\,k}}$, which are contained in the $N \times 1$ vector $\boldsymbol{E}$. The surface

unknowns are the quantities $(\partial E/\partial n)|_m$ on each cell, $m = 1, \ldots, M$. The $M \times 1$ vector $\boldsymbol{U}$ contains these M surface cell derivatives. We can write the resultant system of N equations, each similar to (2), in a state variable form

$$(\boldsymbol{G} + s\boldsymbol{C})\,\boldsymbol{E} = \boldsymbol{BU} \tag{3}$$

where $\boldsymbol{G}$ is an $N \times N$ sparse matrix resulting from the discrete approximation of ∇^2_{xy} while the entries of the diagonal matrix $\boldsymbol{C}$, also $N \times N$, are $(-\sigma\mu)$. The input selector matrix $\boldsymbol{B}$, filled with ones and zeros and of dimensions $N \times M$, introduces the surface cell quantities, such as $(\partial E/\partial n)|_B$, that are adjacent to internal cells lying on the conductor boundary (such as cell (j, k) in Fig. 3) as forcing terms for the system(s). Since our goal is to avoid the computational expense of a volumetric method, we do not want to actually find the electric field or current density at each of the interior nodes. Instead, a transfer function between the discrete values of E_z at the surface boundary and an equivalent surface current density (to be described later) is desired. These surface values of E_z are isolated from the vector $\boldsymbol{E}$ by an output selector matrix $\boldsymbol{L^T}$, filled with ones and zeros and of dimensions $M \times N$, which chooses the interior boundary cells adjacent to the M surface cells to render

$$\boldsymbol{E}_{\text{surface}} \cong \boldsymbol{L^T E} = \boldsymbol{L^T}\left(\boldsymbol{G} + s\boldsymbol{C}\right)^{-1}\boldsymbol{BU}. \tag{4}$$

For example, the field at interior cell (j, k), $E_{z_{j,k}}$, is approximately equal to $E_z|_B$ at surface cell B.

On the surface of the conductor, the tangential magnetic field H_t is related to $\partial E_z/\partial n$ through Maxwell's equation, $\nabla \times E_z = -j\omega B_t$, which leads to

$$\frac{\partial E_z}{\partial n} = -s\mu H_t. \tag{5}$$

Recognizing that H_t has the units of a surface current density, we can replace H_t by an equivalent surface current density $\overline{J} = \hat{n} \times H_t\hat{t} = J_z\hat{z}$; thus, $(\partial E_z/\partial n) = -s\mu J_z$. The vector $\boldsymbol{U}$ in (4) can now be replaced by a vector of surface currents, $\boldsymbol{J}$. Thus, an impedance matrix relationship is established between the electric field at the M surface cells and the equivalent surface currents on these cells

$$\boldsymbol{E}_{\text{surface}} \cong \underbrace{-s\mu\boldsymbol{L^T}\left(\boldsymbol{G} + s\boldsymbol{C}\right)^{-1}\boldsymbol{B}}_{\boldsymbol{Z}}\boldsymbol{J} = \boldsymbol{ZJ}. \tag{6}$$

Matrices $\boldsymbol{L^T}$, $\boldsymbol{G}$, $\boldsymbol{C}$, and $\boldsymbol{B}$ are frequency-independent and need only be computed *once* after the mesh discretizations, $N1$ and $N2$, are chosen based on the maximum frequency of interest. The matrix surface impedance relationship (6) couples together the tangential electric and magnetic fields along a given cross section of the conducting bar. If the cross section of the bar is changing along the axis of the bar, a GSI must be developed for each different cross section. Clearly, the approximation is made here that the electromagnetic field penetration inside the lossy conductor is dominated by the cross-sectional geometry of the conductor, and thus a cross-sectional GSI model suffices. While such an approximation is expected to be a good one for long interconnect structures, it needs to be re-evaluated for short interconnect segments or interconnect discontinuities

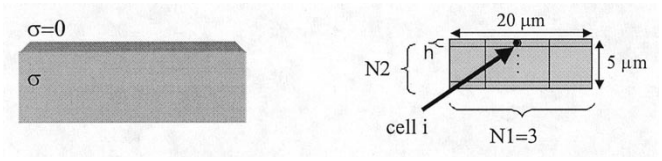

(a) (b)

Fig. 4. (a) A semi-infinite bulk conductor. (b) A conductive bar with finite width and thickness

such as bends, where the surface current density has more than one components. Such cases will be considered in forthcoming papers.

The following sequence of matrix equations indicates the way the eigendecomposition analysis of the matrix $\boldsymbol{C^{-1}G}$ can be used to cast the elements of $\boldsymbol{Z}$ in a computationally convenient, closed-form, and frequency dependent expression

$$\begin{aligned}\boldsymbol{Z} &= -s\mu\boldsymbol{L^T}\left[\boldsymbol{C}\left(\boldsymbol{C^{-1}G} + s\boldsymbol{I}\right)\right]^{-1}\boldsymbol{B}\\ \boldsymbol{Z} &= -s\mu\boldsymbol{L^T}\left(\boldsymbol{C^{-1}G} + s\boldsymbol{I}\right)^{-1}\boldsymbol{C^{-1}B}.\end{aligned} \tag{7}$$

Introducing the eigendecomposition, $\boldsymbol{C^{-1}G} = \boldsymbol{T\Lambda T^{-1}}$, where $\boldsymbol{\Lambda}$ is the diagonal matrix containing the eigenvalues of $\boldsymbol{C^{-1}G}$ we have

$$\begin{aligned}\boldsymbol{Z} &= -s\mu\boldsymbol{L^T}\left(\boldsymbol{T\Lambda T^{-1}} + s\boldsymbol{TT^{-1}}\right)^{-1}\boldsymbol{C^{-1}B}\\ \boldsymbol{Z} &= -s\mu\boldsymbol{L^T T}\left(\boldsymbol{\Lambda} + s\boldsymbol{I}\right)^{-1}\boldsymbol{T^{-1}C^{-1}B}.\\ \text{Let: } \boldsymbol{Q} &= -\mu\boldsymbol{L^T T} \quad \text{and} \quad \boldsymbol{R} = \boldsymbol{T^{-1}C^{-1}B}\end{aligned} \tag{8}$$

$$\boldsymbol{Z} = s\boldsymbol{Q}\left(\boldsymbol{\Lambda} + s\boldsymbol{I}\right)^{-1}\boldsymbol{R} \tag{9}$$

$$\boldsymbol{Z}_{i,j}(s) = s\sum_{n=1}^{N}\frac{\boldsymbol{Q}_{\text{in}}\boldsymbol{R}_{nj}}{s + \boldsymbol{\Lambda}_{nn}}. \tag{10}$$

The pole/residue representation of the elements of $\boldsymbol{Z}$ is readily apparent from the expression in (10), a useful form for including the GSI model into time-domain simulators. Thus, over a cross section of a given interconnect, the surface impedance matrix $\boldsymbol{Z}$ represents the interior regions of a PEEC model in a straightforward and efficient manner, where the equivalent surface currents can be directly incorporated into a PEEC modeling scheme.

III. Global Surface Impedance (GSI) Results

For a conducting half-space, as shown in Fig. 4(a), the surface impedance is well known to be $Z_s = ((1 + j)/s\delta)$. On the other hand, the corners of a bar with finite dimensions, such as in Fig. 4(b), alter this behavior. However, for high enough frequencies, and if the number of thickness divisions, N2, is chosen large enough, the center surface cell indicated in Fig. 4, along the width of the bar, will exhibit approximately the surface impedance behavior of an infinitely wide conducting plane. Thus, as an initial test of the GSI model Fig. 5 was generated in order to verify the accuracy of the model in this limiting case. In addition to model validation, the results displayed in Fig. 5 show that the finite difference cell thickness is sufficiently small enough to model the skin effect if $h < (1/2)\delta_{f_{\max}}$. With this discretization guideline in mind, we proceed next to the numerical

demonstration of the frequency dependent GSI representation of a cross-sectional geometry.

The sample geometry used for the remainder of this section is a 20 μm $\times$ 5 μm copper conductor with $N1 = 20$ and $N2 = 5$, as shown in Fig. 6. The "coupling" between surface elements, or the lack thereof, is most noticeably visible in the 2-D magnitude plots of $|Z_{ij}|$ in Figs. 6 and 7. For a fixed frequency, each of these plots displays the magnitude of the M^2 possible mutual and self-surface cell impedance values. The bright (white) spots along the diagonal, on all three plots, indicate large self-impedances and interactions at the corner cells: 20–21, 25–26, and 45–46. For the high-frequency case (Fig. 7), the self-impedance term is the largest, as expected (notice the bright *diagonal* cells). However, the low-frequency behavior displayed in Fig. 6 is noticeably different. The self-terms are not dominant; the thru-coupling is just as prominent between cells on opposite sides of the conductor including adjacent corners. Notice the *off-diagonal* brightness between cells a) [i: 6–15 and j: 31–40] and b) [i: 17–29 and j: 17–29]. The plot of the mid-frequency surface impedances in Fig. 7 illustrates the less-than obvious transition between uniform volume current distribution and surface-like currents.

It is important to remember that for the generation of these intensity plots, the same mesh and therefore the same system eigenvalues are used, only the variable $s = j\omega = j2\pi f$ changes. The results illustrate that a global surface impedance was formulated in such a way as to capture the *spatial* and *frequency* variations of a lossy conductor as well as separate the interior conductor from its surroundings. The computational benefits of a surface formulation have been previously stated. A closer look at the advantages of an interior–exterior formulation is now in order. The fact that a wire cross section can be characterized, for a range of frequencies, with matrices, $\boldsymbol{L^T}$, $\boldsymbol{G}$, $\boldsymbol{C}$, and $\boldsymbol{B}$, independent of the surrounding geometry, lends itself to the development of component libraries. For a given technology, a set of conductor descriptions would be available, for all frequencies less than $f_{\max}$, independent of their location in a PCB or interconnect structure. This library feature is illustrated in Fig. 8 for a system of conductors embedded in a multilayer board. Additionally, this GSI representation is one that is amenable to inclusion within both surface integral and finite difference-based methods. This abstraction of the conductor behavior from its surroundings and method of computation is extremely advantageous for modularity and portability of the model to other circuit, interconnect, and electromagnetic simulation tools. In the section that follows, the GSI that has just been developed will be used in conjunction with a formulation of the exterior problem in order to determine circuit-like quantities for interconnect structures.

IV. Implementation of GSI in the Electric Field Integral Equation (EFIE)

The global surface impedance that was developed in the previous sections is a relative quantity: it is the ratio between the electric field at the equivalent surface boundary and the equivalent surface current that induces it. In order to determine the *actual* value of the current throughout a conductor's cross-section, the entire domain of interest and system of conductors and dielectrics, such as the one in Fig. 9, must be incorporated into the solution. This section describes a technique that incorporates the GSI models into an electric field integral equation (EFIE) formulation of the exterior problem.

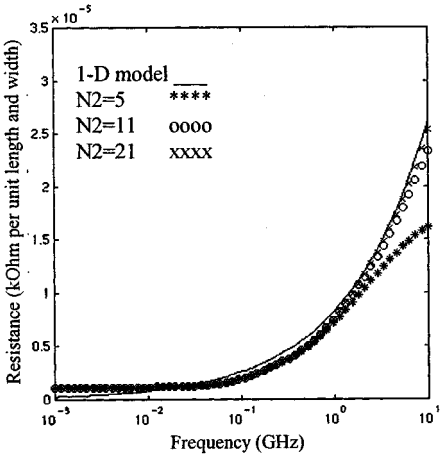

Fig. 5. Validation of the proposed model versus analytical expression for the surface resistance of a semi-infinite conducting space.

Once again, for the purposes of this paper, it is assumed that the interconnect structure of interest involves a set of parallel conductors which poses a constant cross-sectional geometry. Furthermore, the interconnect length is much longer than the cross-sectional dimensions. Consequently, a quasi-TEM transmission line model is appropriate. The EFIE that will be developed will be used to extract the per-unit-length inductance and resistance matrices of the interconnect as functions of frequency.

The longitudinal electric field just outside each of the surface boundaries, E^+_{surface}, can be written as

$$E^+_{\text{surface}} = E_z^{\text{exterior}} + E_z^{\text{incident}}. \tag{11}$$

Since none of the examples in this paper is influenced by an impressed field, E_z^{incident} is set equal to zero; this term is included in (11) for the sake of completeness. The fields just outside the surface boundary are determined from $E_z^{\text{exterior}} = -j\omega A_z - \partial\phi/\partial z$, where $\overline{A} = A_z\hat{z}$ and ϕ are the magnetic vector and electric scalar potential, respectively. Just inside the surface boundary of each conductor, E^-_{surface} is related to the tangential magnetic field through the previously developed GSI matrix, $\boldsymbol{Z}$, for the specific conductor.

Let $\boldsymbol{E_{\text{surface}}}$ and $\boldsymbol{E_{\text{exterior}}}$ denote vectors that contain the values of the electric field, E^-_{surface} and E_z^{exterior}, respectively, at each of the cells on each of the K conductors. Let M_i be the number of surface cells on the ith conductor; then, the length of each one of the vectors $\boldsymbol{E_{\text{surface}}}$ and $\boldsymbol{E_{\text{exterior}}}$ is $N_C = \sum_{i=1}^{K} M_i$. The continuity condition of the tangential electric field, $E^-_{\text{surface}} = E^+_{\text{surface}}$, at all points on each conductor surface requires that $\boldsymbol{E_{\text{surface}}} = \boldsymbol{E_{\text{exterior}}}$. Since the interior region of each conductor is described by a different GSI matrix,

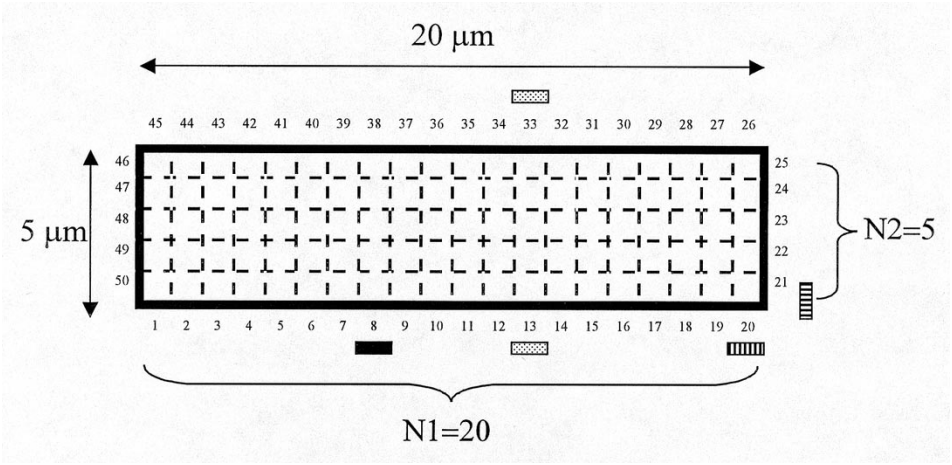

(a)

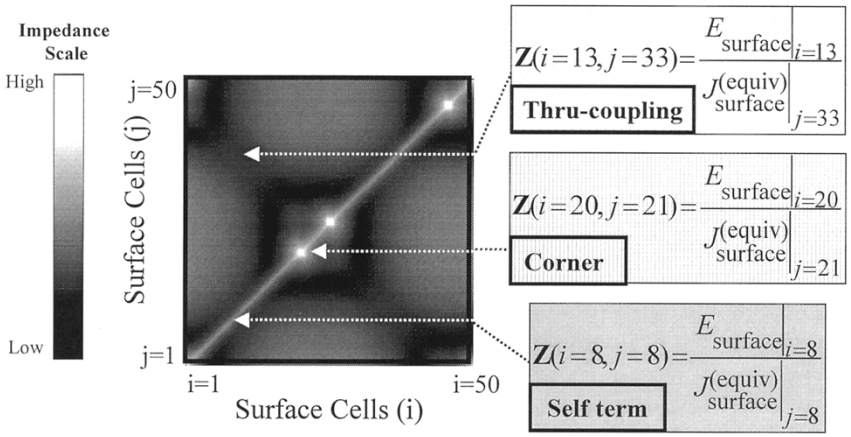

(b)

Fig. 6. (a) Example geometry and (b) $|Zij|$ at Low Frequency: 79.1 MHz.

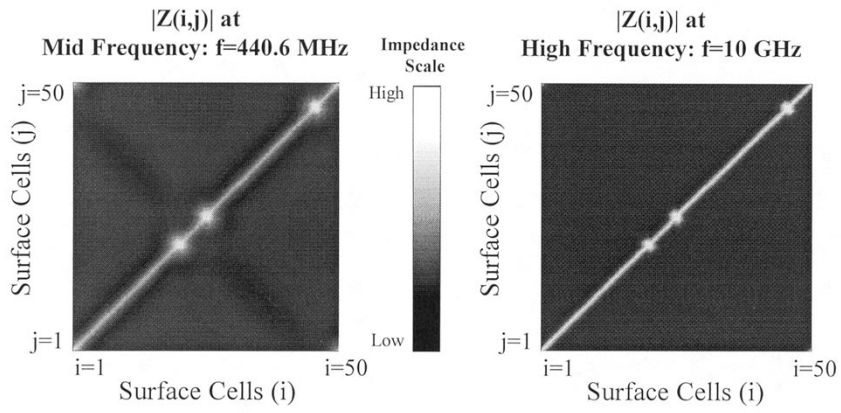

Fig. 7. $|Zij|$ as a function of frequency.

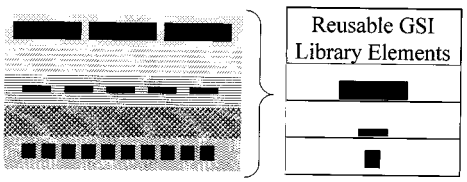

Fig. 8. GSI library elements (one GSI per layer).

$\boldsymbol{Z}$, a block diagonal impedance matrix, $\boldsymbol{Z}_s$, is defined that contains each of the global surface impedances previously derived for each of the K conductors

$$\boldsymbol{Z_S} = \begin{bmatrix} \boldsymbol{Z}^{(k=1)} & & 0 \\ & \ddots & \\ 0 & & \boldsymbol{Z}^{(k=K)} \end{bmatrix}. \tag{12}$$

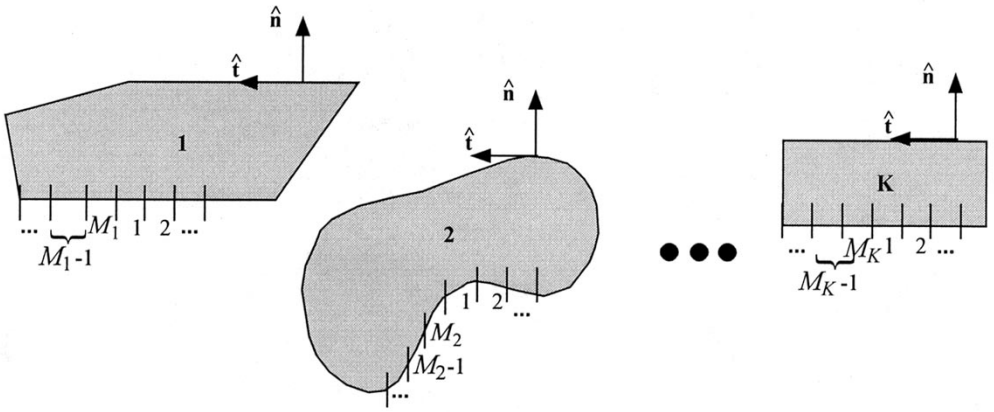

Fig. 9. Cross-sectional view of a system of lossy conductors.

In the following, an integral equation for the tangential electric field exterior to the conductor cross sections is derived. Let J_z denote the equivalent surface electric current on the conductor cross sections. The vector potential $\overline{A}$ is expressed in terms of these surface currents as follows:

$$A_z(\overline{\rho}) = \sum_{k=1}^{K} \frac{\mu}{4j} \int_{C'_k} J_z^{(k)}(\overline{\rho}') H_o^{(2)}\left(\omega\sqrt{\mu\varepsilon}|\overline{\rho} - \overline{\rho}'|\right) dl'. \tag{13}$$

Using the surface cells from part I as pulse basis functions, J_z on conductor k can be approximated as $J_z^{(k)} = \sum_{j=1}^{M_k} J_j^{(k)}$ where each constant $J_j^{(k)}$ has finite support only over the width of surface cell j on conductor k. This simplifies (13) to

$$A_z(\overline{\rho}) = \sum_{k=1}^{K}\sum_{j=1}^{M_k} J_j^{(k)} \frac{\mu}{4j} \int\limits_{\substack{\text{cell } j \text{ on} \\ \text{conductor } k}} H_o^{(2)} \cdot \left(\omega\sqrt{\mu\varepsilon}\left|\overline{\rho} - \overline{\rho}'_j\right|\right) dl'_j. \tag{14}$$

Using the method of moments with point testing at the center of every surface cell on every conductor yields the following system of equations:

$$-j\omega \boldsymbol{A} = \boldsymbol{Z}_{\mathrm{MoM}} \boldsymbol{J} \tag{15}$$

where $\boldsymbol{A}$ contains the vector potential response at each test point "i." The interactions between cells (i, j) found in $\boldsymbol{Z}_{\mathrm{MoM}}$ are approximated in the same fashion as in Harrington [7].

To complete the development of the matrix equation that describes the tangential electric field on the exterior of the discretized surfaces of the conductor cross sections, the term $\partial\phi/\partial z$ must be included. For the 2-D problem of interest it is well known that $\partial\phi/\partial z$ is constant for each conductor [3]. If $\partial\phi/\partial z$ is arbitrarily specified for each conductor, it serves as a potential difference per-unit-length, i.e., a voltage source, which drives the problem. Alternatively, one may choose to constrain the net current that flows through each conductor. This essentially implies the use of a current source, in which case $\partial\phi/\partial z$ is an additional unknown to be determined. For reasons that will be discussed later, the latter approach is used. More specifically, $J_z^{(k=K)} = \sum_{j=1}^{M_{k=K}} J_j^{(k=K)} = 1$ for one conductor, and $J_z^{(k\neq K)} = \sum_{j=1}^{M_{k\neq K}} J_j^{(k\neq K)} = 0$ for all other conductors. Imposing the continuity of the tangential electric and magnetic fields at the conductor surface leads to the desired integral equation. The relevant mathematical development is summarized in the following:

a) $\boldsymbol{E}_{\mathbf{surface}} = \boldsymbol{E}_{\mathbf{exterior}}$

b) $J_z^{(k=K)} = \sum_{j=1}^{M_{k=K}} J_j^{(k=K)} = 1$

and

$$J_z^{(k\neq K)} = \sum_{j=1}^{M_{k\neq K}} J_j^{(k\neq K)} = 0 \tag{16}$$

a) $\boldsymbol{Z_s J} = -j\omega \boldsymbol{A_z} - \partial\phi/\partial z$

$\boldsymbol{Z_s J} = \boldsymbol{Z}_{\mathrm{MoM}} \boldsymbol{J} - \partial\phi/\partial z$

b) $\underbrace{\begin{bmatrix} \overline{1}_{1\times M_1} & \overline{0}_{1\times M_1} & \cdots & \overline{0}_{1\times M_K} \\ & \ddots & & \\ \overline{0}_{1\times M_1} & \cdots & \overline{0}_{1\times(M_K-1)} & \overline{1}_{1\times M_K} \end{bmatrix}}_{\boldsymbol{V}}$

$$\boldsymbol{J} = \begin{bmatrix} 0 \\ \vdots \\ 1 \end{bmatrix} \tag{17}$$

$$\begin{bmatrix} \underbrace{[\boldsymbol{Z}_{\mathrm{MoM}} - \boldsymbol{Z_s}]}_{\boldsymbol{Z'}} & \begin{bmatrix} \overline{0}_{(M_1\times 1)} \\ \vdots \\ \overline{1}_{(M_K\times 1)} \\ 0 \end{bmatrix} \\ \boldsymbol{V} & \end{bmatrix} \begin{bmatrix} \boldsymbol{J} \\ \\ -\left.\dfrac{\partial\phi}{\partial z}\right|_{k=K} \end{bmatrix} = \begin{bmatrix} \overline{0}_{(N_C\times 1)} \\ \\ 0 \\ \vdots \\ 1 \end{bmatrix}. \tag{18}$$

In (18), there are $(N_C + K)$ unknowns. The extra K equations are provided by constraint b) in (16). $[\boldsymbol{J}^{(1)} \ \cdots \ \boldsymbol{J}^{(K-1)} \ J_{j=1}^{(K)} \cdots J_{j=(M_K)-1}^{(K)} \ -\partial\phi_{k=K}/\partial z]^T$. This completes the development of the system of equations needed for the calculation of the equivalent surface currents on the surfaces of the cross sections of the conductors. If the specific field distributions within a conductor are desired, they can be found using the original internal models from Section II

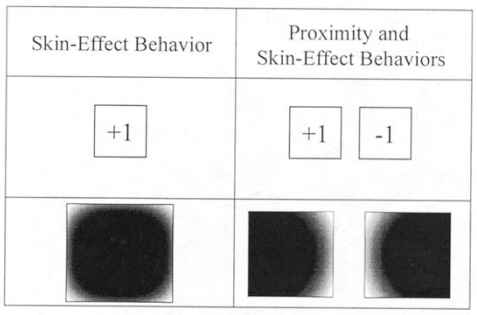

Fig. 10. Demonstration of the skin-effect behavior of a lossy (isolated) conductor and lossy conductors in close proximity.

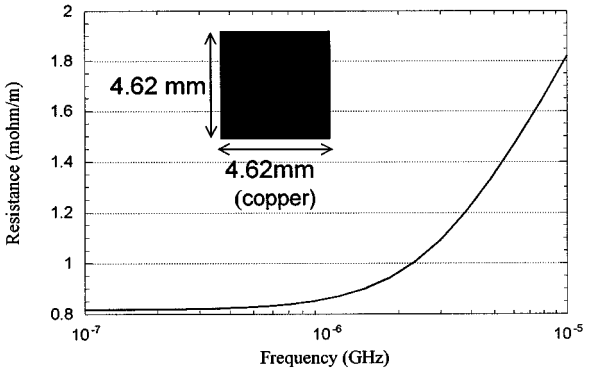

Fig. 11. Resistance of isolated square wire.

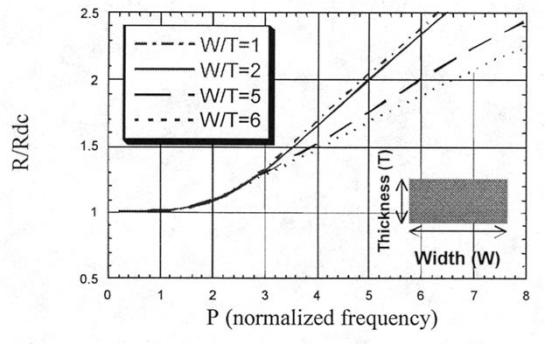

Fig. 12. Normalized resistance versus normalized frequency, $P = \sqrt{2\mu\sigma f A}$, for various conductor aspect ratios.

and the equivalent surface currents found in J. The entire procedure is summarized below.

I) For each conductor cross section, compute the GSI matrix in the form of (10), if it does not already exist in the library of conductor cross sections.

II) Incorporate the multiconductor GSI representation, $\boldsymbol{Zs}$, in the electromagnetic solver of choice for the exterior problem.

III) Solve for the equivalent surface currents on the cross sections of the coupled conductors.

IV) Compute resistance and inductance per-unit-length (p.u.l.) as described in the following section. One can also determine the interior electric field $\boldsymbol{E} = \boldsymbol{ZJ}$.

V. Results

It is important to realize that since both the interior and exterior of the conductor are rigorously modeled and the proper boundary conditions are enforced, both local (internal) and global (external) electrical effects are modeled accurately. In Fig. 10, a single GSI matrix is used to determine the current distributions for both a single and coupled two-line geometry. Column one illustrates how the current density exhibits a surface like distribution when the skin-effect behavior is dominant. If the *same* GSI model for each cross section is then used in the two-conductor case of column two, the preferential crowding of the current on the side next to the other conductor caused by the proximity effect (a global phenomenon) is clearly visible along with the skin-effect behavior.

Transmission line-type quantities such as resistance and inductance per unit length are easily computed from field and current quantities as follows:

$$R = \frac{2P_d}{|I|^2} = \frac{\iint ds|J_z|^2}{\sigma\left|\iint dsJ_z\right|^2}$$

$$L = \frac{4W_m}{|I|^2} = \frac{\mathrm{Re}\left\{\iint dsA_zJ_z^*\right\}}{\left|\iint dsJ_z\right|^2}. \tag{19}$$

The results that follow can be compared with the results presented in Tsuk and Kong [3]. Their work is benchmarked along with results that exclusively use either surface or volume based techniques. All of the results in this section were generated by selecting $N1$ and $N2$ to meet the discretization condition that was validated in Section III: $h < (1/2)\delta_{f_{\max}}$. Depending on the resources available, a memory storage limit will be reached as $f_{\max}$ of a frequency response is increased. However, nonuniform gridding or formulation in terms of entire domain basis functions can be used to address this problem. When comparing our results to results from the literature, it is important to emphasize the primary attribute of the GSI model. The fact that the GSI representation avoids the development of a system of coupled integral equations allows for repeated use of a conductor (cross section) without introducing new models for each occurrence (see Fig. 8). Thus, the number of surface cells needed for the development of a GSI becomes a secondary issue. In fact, if full domain basis functions are used, especially those that mimic the singular behavior of the surface current-density at conductor edges, a GSI can be generated in a very efficient fashion, independent of the discretization size chosen for the exterior problem.

Our first example is the isolated copper conductor of Fig. 11. The conductivity throughout its square cross section is $\sigma = 5.72E7$ $(\Omega\text{-m})^{-1}$. Using 20 divisions per side, our results shown in Fig. 11 are nearly identical to the results in [3] (not shown). To illustrate the accuracy of our GSI model, independent of a conductor's aspect ratio, the thickness of the conductor used in Fig. 11 was varied in order to simulate the conductor aspect ratios presented in Fig. 12. Although it was not necessary to do so, the ratio, $N1/N2$, between the number of divisions along the

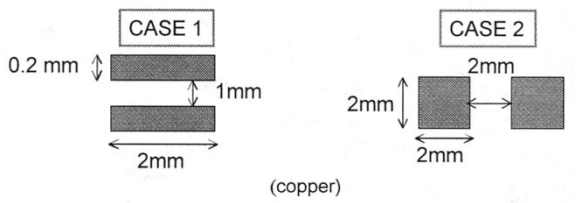

Fig. 13. Cross-sectional geometries of a two-conductor system where one of the conductors is used as the return path.

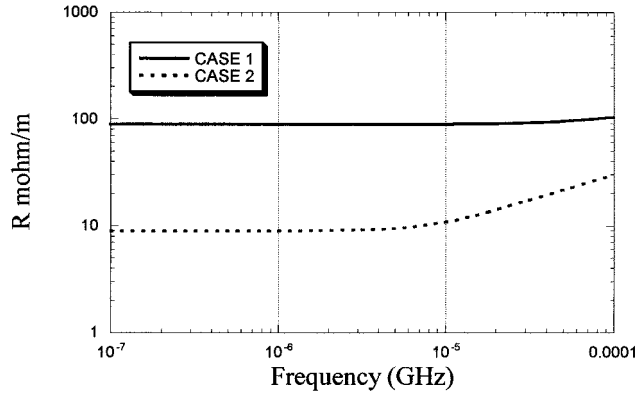

Fig. 14. Per-unit-length resistance of the two-conductor lines of Fig. 13.

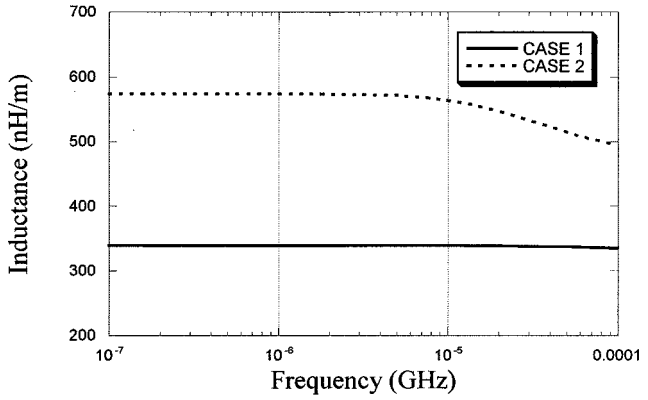

Fig. 15. Per-unit-length inductance of the two-conductor lines of Fig. 13.

conductor's width and thickness (respectively) were scaled to equal each specific (W)idth/(T)hickness ratio. While the conductivity was held constant at $\sigma = 5.72E7\,(\Omega\text{-m})^{-1}$, each curve was normalized to the Rdc value for each specific W/T ratio. A direct comparison can be made between Fig. 12 and results presented in [8], where A is equal to the conductor's cross-sectional area. Each of the curves shown in Fig. 12 closely agrees with the corresponding result found in [8].

The symmetric coupled interconnect geometries in Fig. 13 are also examined by Tsuk and Kong. As with the single conductor results, the correspondence between the results of the GSI model and those of other, more computationally expensive methods, are practically identical. Figs. 14 and 15 display the frequency dependent behavior of the resistance and inductance for the two geometries of Fig. 13 calculated using GSI models.

VI. Conclusions and Future Work

In summary, a GSI was developed which accurately and efficiently models the quasistatic electromagnetic behavior of a 2-D lossy conductor. Since the interior of the conductor cross section is discretized and incorporated into the formulation of the GSI model, it eliminates the need for a high-frequency volume filament approach. The modification was shown to accurately capture the spatial and frequency dependent behaviors associated with *both* the skin and proximity effects. More significantly, the GSI matrix $\boldsymbol{Z}$ is compatible with both integral equation-based and finite method-based modeling of interconnect structures for the purposes of global signal integrity and interference analysis. This is possible due to the abstraction of the GSI model from its physical and computational settings. The GSI representation is also conducive to building a library of conductor element models where the GSI serves as a rigorous surface impedance description of the conductor interior. The pole-residue form of the elements of the GSI matrix is directly compatible with the recursive convolution schemes commonly used for the purpose of a computationally efficient description of frequency-dependent effects. The cost of using the GSI model in transient simulations is directly related to the number of poles used in the pole–zero representation. This cost can be controlled by utilizing model order-reduction techniques [9].

References

[1] H. A. Wheeler, "Formulas for the skin effect," *Proc. IRE*, vol. 30, pp. 412–424, Sept. 1942.
[2] C. S. Yen, Z. Fazarinc, and R. L. Wheeler, "Time-domain skin-effect model for transient analysis of lossy transmission lines," *Proc. IEEE*, vol. 70, pp. 750–757, July 1982.
[3] M. J. Tsuk and A. J. Kong, "A hybrid method for the calculation of the resistance and inductance of transmission lines with arbitrary cross sections," *IEEE Trans. Microwave Theory Tech.*, vol. 39, pp. 1338–1347, Aug. 1991.
[4] S. Kim, B. T. Lee, E. Tuncer, and D. Neikirk, "Effective internal impedance method for series impedance calculation of lossy transmission lines: Comparison to standard impedance boundary condition," IEEE Trans. Microwave Theory Tech., submitted for publication.
[5] A. E. Ruehli, "Equivalent circuit models for three dimensional multiconductor systems," *IEEE Trans. Microwave Theory Tech.*, vol. 22, pp. 216–221, Mar. 1974.
[6] M. Kamon, N. Marques, L. M. Silveira, and J. White, "Generating reduced order models via PEEC for capturing skin and proximity effects," in *Electrical Performance of Electronic Packaging* West Point, NY, Oct. 1998, pp. 259–262.
[7] R. Harrington, *Field Computation by Moment Methods.* New York: IEEE Press, 1993.
[8] R. Faraji-Dana and Y. L. Chow, "The current distribution and AC resistance of a microstrip structure," *IEEE Trans. Microwave Theory Tech.*, vol. 38, pp. 1268–1277, Sept. 1990.
[9] A. Odabasioglu, M. Celik, and L. T. Pileggi, "PRIMA: Passive reduced-order interconnect macromodeling algorithm," *IEEE Trans. Computer-Aided Design*, vol. 17, pp. 645–654, Aug. 1998.

Karen M. Coperich, photograph and biography not available at time of publication.

Albert E. Ruehli (M'65–SM'74–F'84), photograph and biography not available at time of publication.

Andreas Cangellaris (M'86–SM'97–F'00), photograph and biography not available at time of publication.